Article

Development of 1-(4-(Substituted)piperazin-1-yl)-2-((2-((4-methoxybenzyl)thio)pyrimidin-4-yl)oxy)ethanones That Target Poly (ADP-Ribose) Polymerase in Human Breast Cancer Cells

Suresha N. Deveshegowda [1,†], Prashant K. Metri [1,†], Rashmi Shivakumar [1], Ji-Rui Yang [2], Shobith Rangappa [3], Ananda Swamynayaka [4], Muthu K. Shanmugam [5], Omantheswara Nagaraja [4], Mahendra Madegowda [4], Priya Babu Shubha [6], Arunachalam Chinnathambi [7], Sulaiman Ali Alharbi [7], Vijay Pandey [2], Kwang Seok Ahn [8,9], Peter E. Lobie [2,10,11,*] and Basappa Basappa [1,*]

[1] Laboratory of Chemical Biology, Department of Studies in Organic Chemistry, University of Mysore, Manasagangotri, Mysore 570006, India; sureshand92@gmail.com (S.N.D.); prashant.metri@gmail.com (P.K.M.); rashmis1410@gmail.com (R.S.)

[2] Tsinghua Berkeley Shenzhen Institute, Tsinghua Shenzhen International Graduate School, Tsinghua University, Shenzhen 518055, China; yang.jirui@sz.tsinghua.edu.cn (J.-R.Y.); vijay.pandey@sz.tsinghua.edu.cn (V.P.)

[3] Adichunchanagiri Institute for Molecular Medicine, BG Nagara, Nagamangala Taluk, Mandya 571448, India; shobithrangappa@gmail.com

[4] Department of Studies in Physics, University of Mysore, Manasagangotri, Mysore 570006, India; anandas@physics.uni-mysore.ac.in (A.S.); omantheswara@physics.uni-mysore.ac.in (O.N.); mahendra@physics.uni-mysore.ac.in (M.M.)

[5] Department of Pharmacology, Yong Loo Lin School of Medicine, National University of Singapore, Singapore 117600, Singapore; phcsmk@nus.edu.sg

[6] Department of Studies in Chemistry, University of Mysore, Manasagangotri, Mysore 570006, India; priyabs_chem@yahoo.com

[7] Department of Botany and Microbiology, College of Science, King Saud University, Riyadh 11451, Saudi Arabia; carunachalam@ksu.edu.sa (A.C.); sharbi@ksu.edu.sa (S.A.A.)

[8] KHU-KIST Department of Converging Science and Technology, Kyung Hee University, Seoul 02447, Korea; ksahn@khu.ac.kr

[9] Department of Science in Korean Medicine, Kyung Hee University, 24 Kyungheedae-ro, Dongdaemun-gu, Seoul 02447, Korea

[10] Institute of Biopharmaceutical and Health Engineering, Tsinghua Shenzhen International Graduate School, Tsinghua University, Shenzhen 518055, China

[11] Shenzhen Bay Laboratory, Shenzhen 518055, China

* Correspondence: pelobie@sz.tsinghua.edu.cn (P.E.L.); salundibasappa@gmail.com (B.B.)

† These authors contributed equally to this work.

Abstract: A number of uracil amides cleave poly (ADP-ribose) polymerase and therefore novel thiouracil amide compounds were synthesized and screened for the loss of cell viability in a human-estrogen-receptor-positive breast cancer cell line. The synthesized compounds exhibited moderate to significant efficacy against human breast cancer cells, where the compound **5e** IC_{50} value was found to be 18 μM. Thouracil amide compounds **5a** and **5e** inhibited the catalytical activity of PARP1, enhanced cleavage of PARP1, enhanced phosphorylation of H2AX, and increased CASPASE 3/7 activity. Finally, in silico analysis demonstrated that compound **5e** interacted with PARP1. Hence, specific thiouracil amides may serve as new drug-seeds for the development of PARP inhibitors for use in oncology.

Keywords: PARPi; breast cancer; thiouracil amides; apoptosis

1. Introduction

Poly (ADP-ribose) polymerase (PARP) is an enzyme which catalyzes poly ADP-ribosylation of specific target proteins. The PARP family contains 17 enzymes, among which PARP1 is the most abundant and widely studied [1–3]. It is involved in a number of

cellular functions, such as DNA repair, recombination, and gene transcription [4]. More than 70 PARP inhibitors are undergoing clinical trials, some of which are approved by the U.S. Food and Drug Administration, for instance, Niraparib, Olaparib, Talazoparib, and Rucaparib [5–8]. Evidence suggests that PARP plays an important role in cancer cell signaling, chromatin regulation, and metastatic processes that involve cell survival, migration, and invasion [9]. For example, in estrogen-receptor-positive (ER+) breast cancer, PARP regulates the transcriptional activity of ERα, and is reported to be downstream of ER-dependent transcriptional responses [10].

A number of PARP1 inhibitors (PARPi) have been reported; however, the commonly used example of a PARPi, 3-substituted benzamide (3-AB) was a nicotinamide analog [11]. Generally, benzamides inhibit PARP due to their structural analogy to NAD and therefore compete with NAD at the catalytic domain of PARPs [12]. Despite their ability to elucidate the function of PARP, benzamides fail to show PARP inhibitory activity in nanomolar ranges and exhibited off-target effects that precluded their clinical evaluation. Additionally, indazole amides have been shown to be PARP1 inhibitors [13].

Conversely, substituted uracil derivatives have been reported as potent inhibitors of PARP by inhibiting thymidylate synthesis as well as basal excision repair (BER) mechanisms [14,15]. Indeed, thiouracil- or uracil-based compounds are known to act on cancer cells via an anti-folate mechanism, where its misincorporation is genotoxic and eventually contributes to DNA double-strand break and ultimately cell death [16].

The synthesis, characterization, and efficacy of new thiouracil amides were therefore investigated herein and found a lead compound **5e** that inhibits both PARP1 catalytic activity and breast cancer cell viability.

2. Results and Discussion

2.1. Chemical Synthesis of Novel Thiouracil Amides

The synthesis of novel thiouracil derivatives and their characterization is herein reported. In the present investigation, regioisomeric 2-thiopyrimidine acetic acids were utilized as a template to prepare a library of novel amides with various amines, as described in Scheme 1.

The synthetic sequence commenced by reacting 2-thiouracil with substituted benzyl derivative to afford S-benzylated products. The phenolic hydroxyl group in S-benzylated products was treated with tert-butyl acetate to afford tert-butyl esters which were subjected to hydrolysis to afford 2-thiopyrimidine acetic acid. The acid so obtained was coupled with various amines to afford amides **5a–5l**. The structures of these newly synthesized amide derivatives were confirmed by ^{1}H NMR, ^{13}CNMR, and LC/MS analysis.

2.2. Novel Thiouracil Derivatives Produce Loss of Breast Cancer Cell Viability

The synthesized compounds were screened for loss of cell viability using the ER+ breast cancer cell line by Alamar Blue cell viability assays [17–22]. The compounds were dissolved in DMSO and cells were treated in a dose-dependent manner for 72 h. Amongst the tested amides, compounds **5a**, **5b**, **5e**, and **5f** showed significant loss of cell viability with IC_{50} values of 22.68, 25.71, 18.23, and 29.34 μM, respectively, as shown in Figure 1 and Table 1. The other compounds tested from the series exhibited less efficacy. The thiouracil amides possessing tolyl or halophenyl groups displayed significant loss of breast cancer cell viability, according to studies on the structure–activity relationship of this library of compounds. Furthermore, the loss of cell viability produced by the lead compounds (**5a**, **5e**) was compared with Olaparib using immortalized but otherwise normal human mammary epithelial cells (MCF-10A) as an indicator of effect on normal cells. It was observed that these compounds produced loss of cell viability of MCF-10A cells with IC_{50} values of 46.9 and 52.3 μM for compounds **5a** and **5e**, respectively, which were comparable to Olaparib, where IC_{50} was observed to be 57.3 μM (Supplementary Materials).
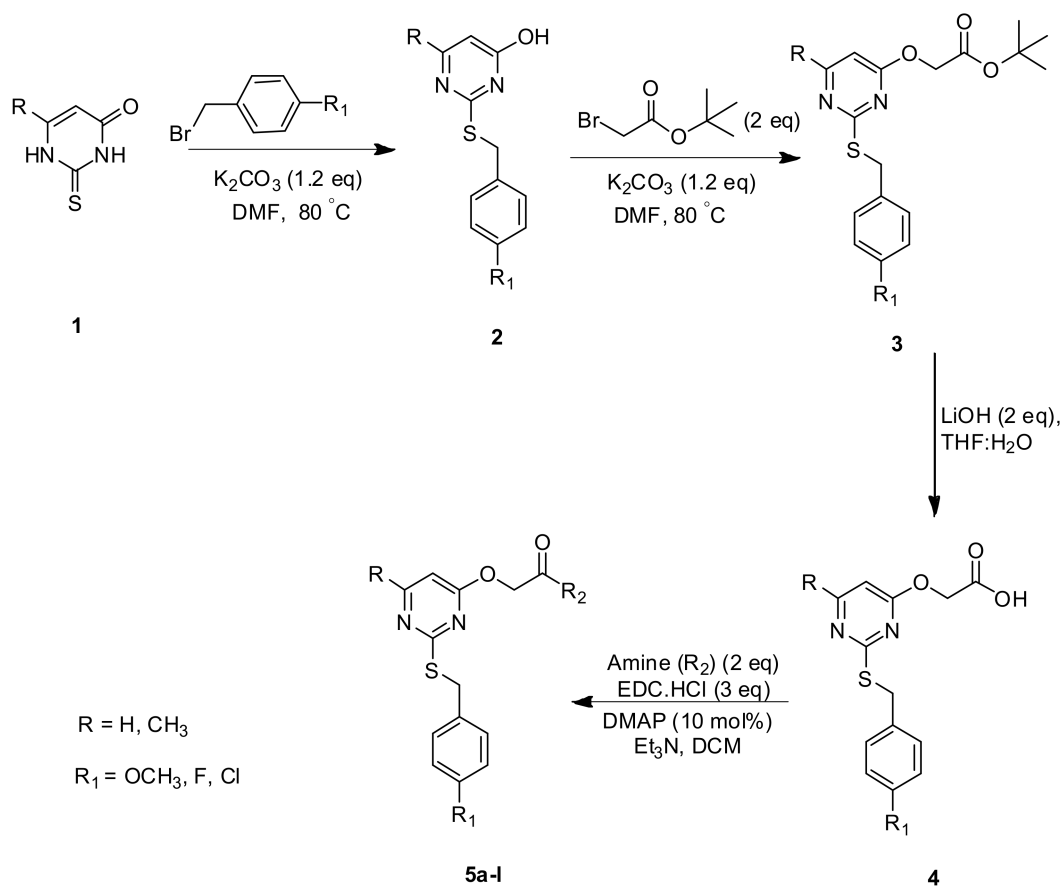
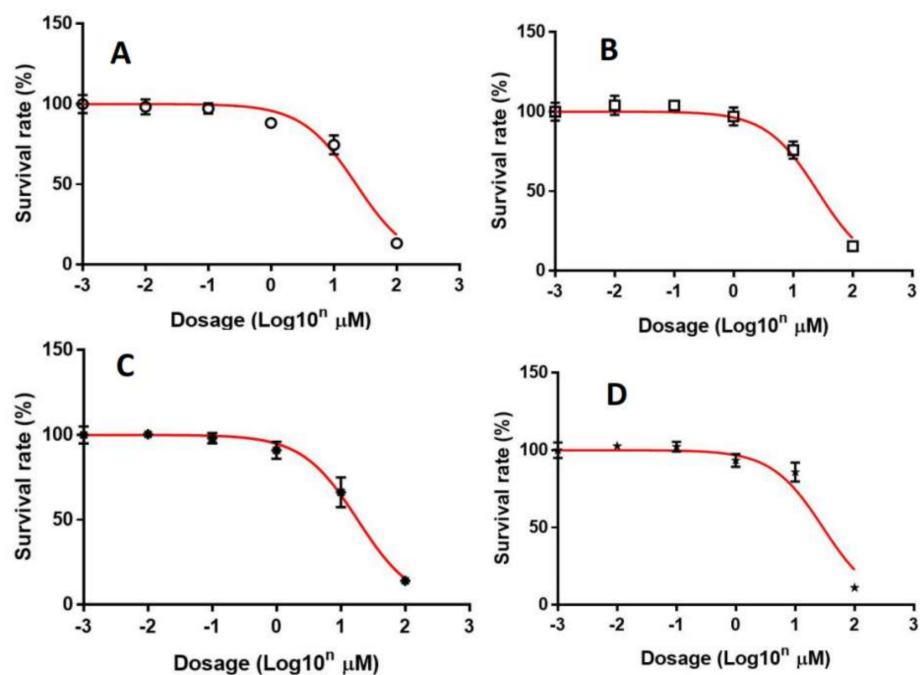**Scheme 1.** Synthesis of thiouracil containing amide derivatives.

Figure 1. Loss of MCF-7 cell viability produced by compounds **5a**, **5b**, **5e**, and **5f**. MCF-7 were exposed to **5a** (**A**), **5b** (**B**), **5e** (**C**), and **5f** (**D**) for 72 h and the viability of cells was analyzed by Alamar Blue assays. The results are presented as mean ± S.E.M. of triplicate determinations.

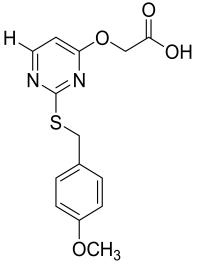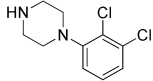**Table 1.** Thiouracil amides structure and their cytotoxicity results tabulated.
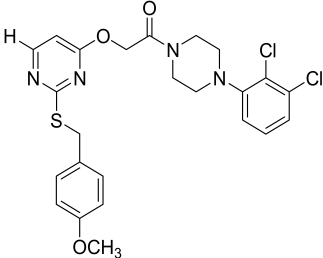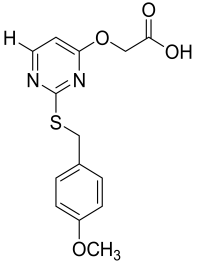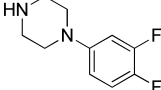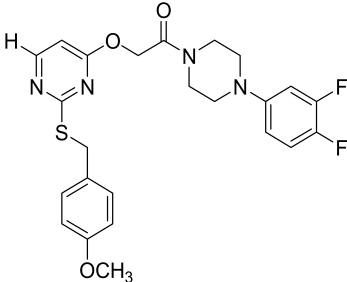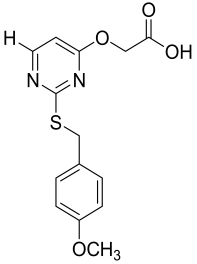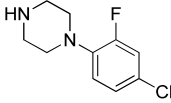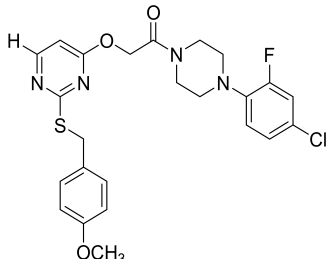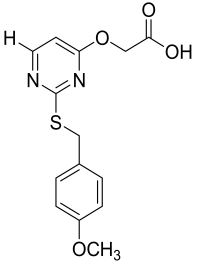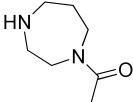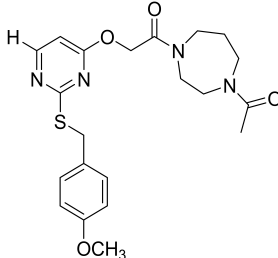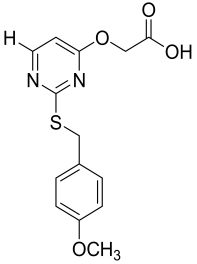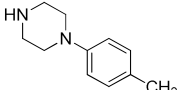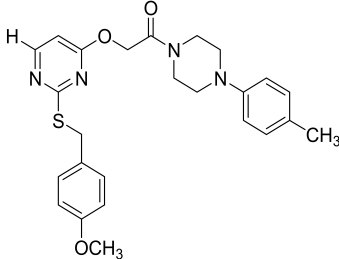
Entry	Acid	Amine (R$_2$)	Structure	MCF-7 (IC$_{50}$ μM)
5a				**22.68**
5b				**25.71**
5c				49.72
5d				106.20
5e				**18.23**

Table 1. *Cont.*
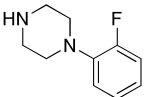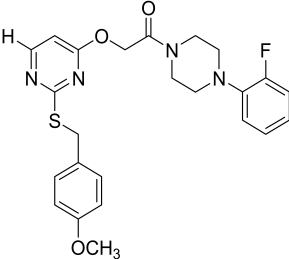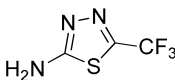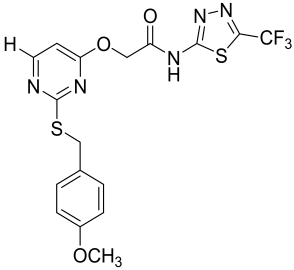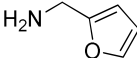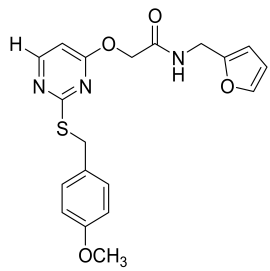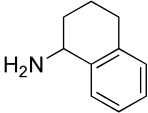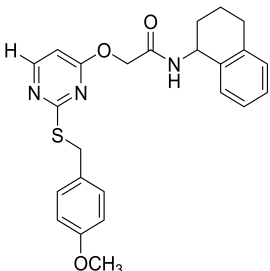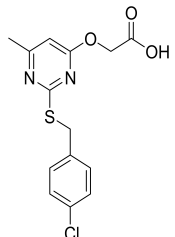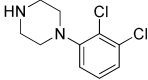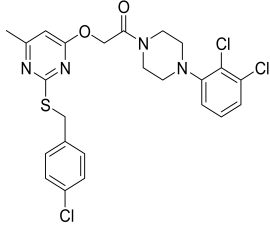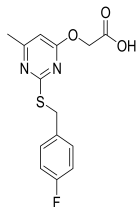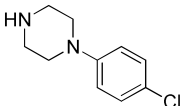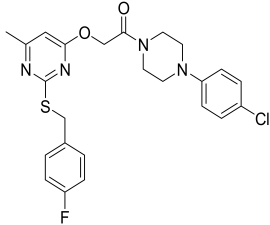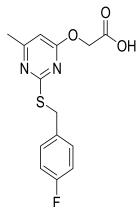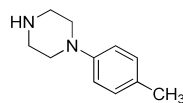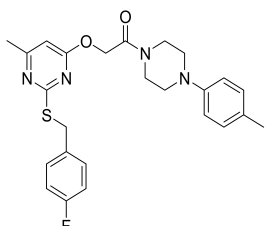
Entry	Acid	Amine (R$_2$)	Structure	MCF-7 (IC$_{50}$ μM)
			Lead molecule	
5f				29.34
5g				39.27
5h				68.18
5i				31.14
5j				41.38

Table 1. *Cont.*

Entry	Acid	Amine (R$_2$)	Structure	MCF-7 (IC$_{50}$ μM)
5k				>100
5l				>100
	Olaparib			**3.28**

2.3. Compounds *5a* and *5e* Inhibit PARP1 Activity

Compounds **5a** and **5e** were tested for their capacity to inhibit PARP1 catalytic activity [23]. Compounds **5a** and **5e** were used at concentrations of 0.01, 0.1, 1, 10, and 100 μM. Compound **5a** was found to inhibit the catalytical activity of PARP1 0.5, 15.6, 29.8, 70.3, and 85.8% at the tested concentrations, whereas compound **5e** inhibited PARP1 activity at 1.3, 2.0, 20.6, 53, and 82.1%. 3-aminobenzamide inhibited PARP1 activity by 1.7, 3, 48.7, 61.9, and 87.2% at the tested concentrations, respectively (Figure 2).
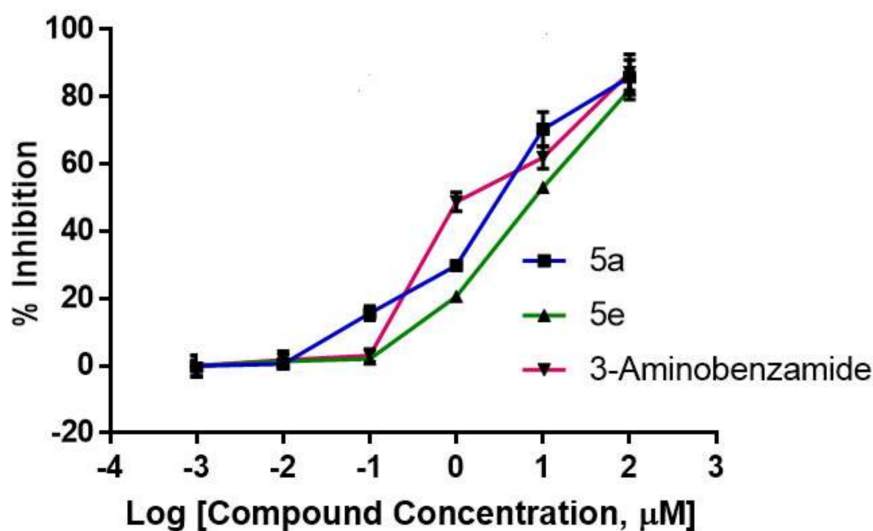
Figure 2. Compounds **5a**, **5e**, and 3-aminobenzamide inhibited the PARP1 catalytic activity. Graphical representation of the inhibition of the catalytic activity of PARP1 by indicated compounds (*n* = 3). Data are expressed as mean ± SEM.

2.4. Lead Compounds Increased PARP1 Cleavage, Phospho-H2AX Levels, and Caspase-3/7 Activation in MCF-7 Cells

The effects of compounds **5a**, **5e**, and Olaparib on the cleavage of PARP1 in MCF-7 cells were performed using the previously reported protocol [24–27]. MCF-7 cells were incubated with **5a, 5e,** or Olaparib at the indicated concentrations. As observed in Figure 3A, treatment of breast cancer cells with either compound **5a** or **5e** produce PARP cleavage comparable to that observed with Olaparib.
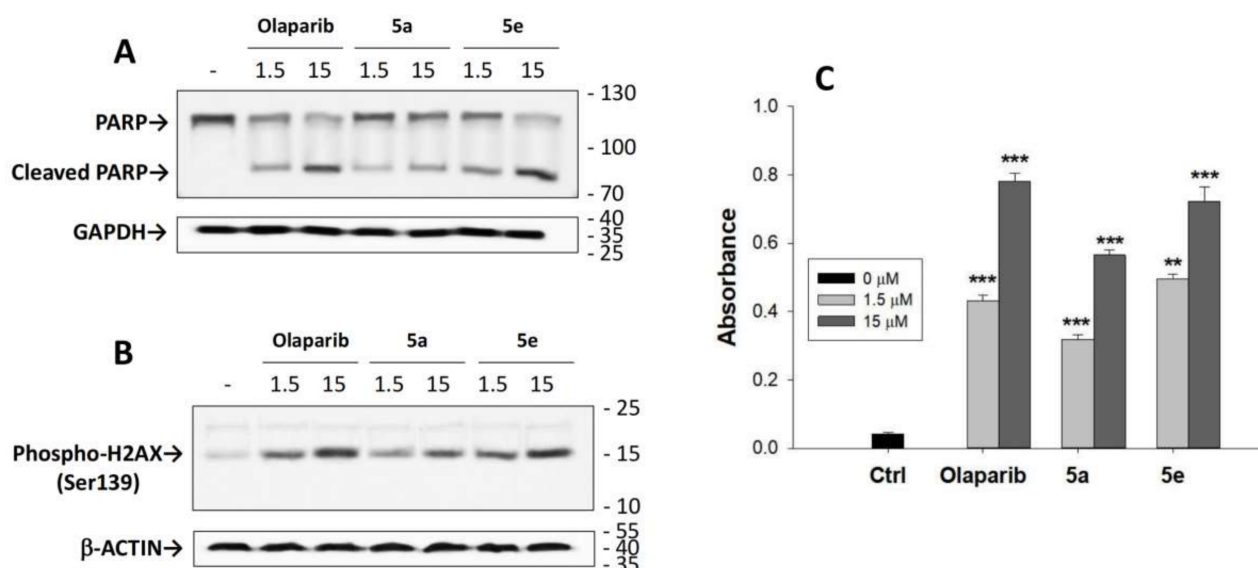
Figure 3. Compounds **5a**, **5e**, and Olaparib cleave PARP1 (**A**) and increase phosphorylation of H2A-X (**B**) and CASPASE-3/7 activity (**C**) in MCF-7 cells. MCF-7 cells were treated with or without compounds **5a, 5e**, or Olaparib at the indicated concentrations. The respective protein bands were detected by Western blot analysis. GAPDH or β-ACTIN were used as input controls. Data are expressed as mean ± SEM. ** $p \leq 0.01$; *** $p \leq 0.001$.

Phosphorylation of Ser139 in H2AX is an indicator of cellular DNA damage which occurs upon PARP inhibition [28]. For example, Olaparib has been reported to enhance H2AX phosphorylation in various cancer cell lines [29]. Therefore, the effect of compounds **5a** or **5e** or Olaparib on the level of p-H2AX in MCF-7 cells was determined (Figure 3B). It was observed that compounds **5a** and **5e** increased phosphorylation of H2AX in MCF-7 cells comparable to that observed with Olaparib.

The effect of compounds **5a** or **5e** and Olaparib on CASPASE 3/7 activity was also examined as an indicator of apoptosis [30–32]. Hence, CASPASE 3/7 activity was determined after treatment of breast cancer cells with compounds **5a** or **5e** or Olaparib. Both compounds **5a** and **5e** increased CASPASE 3/7 activity in a dose-dependent manner and were roughly comparable to that observed with Olaparib (Figure 3C).

2.5. Density Functional Theory (DFT) Calculations

DFT calculations were performed to understand the stability of compound **5e** in the catalytical grove of PARP1 [33–35]. According to the frontier molecular orbital theory, the highest occupied molecular orbitals (HOMO) and lowest unoccupied molecular orbitals (LUMO) are the most effective factors in bioactivity. HOMO has the priority to provide electrons, while LUMO can accept electrons. Thus, studies on the frontier orbital energy may provide useful information of the biological mechanism [36]. The B3LYP level of theory was used to calculate the energy of HOMO, LUMO, and the E_{gap} value, which were used to study the chemical stability, molecular polarizability, and chemical softness or hardness of compound **5e**. The distribution and energy levels of the HOMO and LUMO for **5e** are shown in Figure 4. The positive phase of the molecule is represented in red color,

whereas the negative phase is in green color. It is clear from the plots that the HOMO is localized on the 1-(4-methylphenyl)piperazine ring. In contrast, LUMO is delocalized on the methoxypyrimidine ring and sulfur atom. The HOMO and LUMO values of conformer **5e** are −5.740 eV and −1.124 eV, respectively, and the energy separation between HOMO and LUMO is 4.615 eV. The stabilization and interactions of the compounds with the catalytic site of the enzyme may be explained by global reactivity descriptors and are represented in Table 2. The ionization energy can be expressed as $I = -E_{HOMO} = 5.740$ eV, and the electron affinity can be expressed as $A = -E_{LUMO} = 1.124$ eV. Hardness represents the resistance of a chemical system against the deformation of the electron cloud under the slight interference encountered in the chemical process and can be expressed as $\eta = (E_{LUMO} - E_{HOMO})/2$. The hardness and softness values of the **5e** molecule are 2.307 eV and 0.216 e^{-1} V^{-1}, respectively. With the smaller value of softness, the molecule is chemically stable.
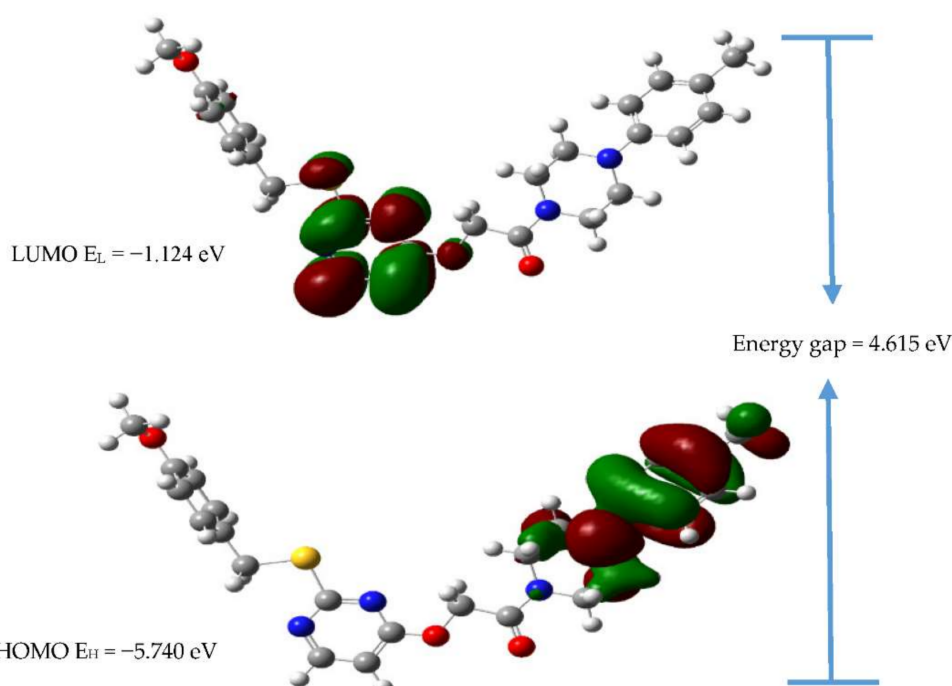
Figure 4. The HOMO and LOMO of molecule **5e** obtained by the DFT/B3LYP/6-31+G (d,p) method.

Table 2. The calculated FMOs and global chemical reactivity descriptors.

Orbital Energy	DFT/B3LYP
E_{HOMO}	−5.740 eV
E_{LUMO}	−1.124 eV
$\Delta E_{LUMO - HOMO}$	4.615 eV
Ionization potential (I)	5.740 eV
Electron affinity (A)	1.124 eV
Hardness (η)	2.307 eV
Softness (S)	0.216 eV^{-1}
Chemical potential (μ)	−3.432 eV
Electronegativity (χ)	3.432 eV
Electrophilicity (ψ)	2.553 eV

MEPs are fundamental measures of the interaction strength of the nearby charges, nuclei, and electrons at a particular position, thus enabling visualization of the charge distribution and charge-related characteristics of molecules. To facilitate interpretation of the electrostatic potential data, a visual representation with a chromatogram is used. The B3LYP/6-31+G (d,p) level of theory was used to study the molecular electrostatic potential

in the intermolecular interaction region of conformer **5e**. The resulting MEP map with a range of -6.351×10^{-2}–6.351×10^{-2} depicts its potential distribution (see Figure 5). The O atom of the C=O bond of molecule **5e** is surrounded by a positive charge, indicating a possible nucleophilic attack site. Furthermore, a negatively charged region is located on the hydrogen atoms of the piperazine ring, indicating a probable electrophilic attack site.
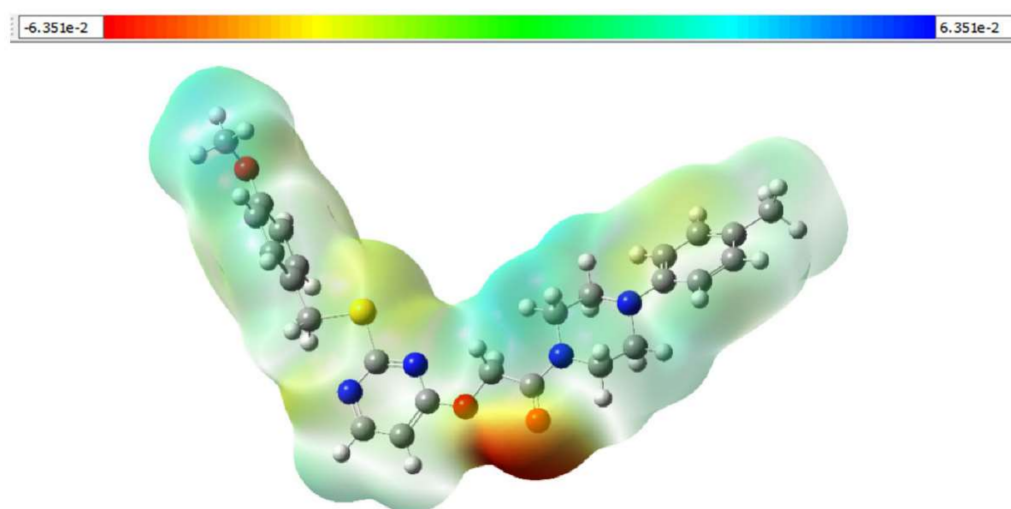
Figure 5. Molecular electrostatic potential surfaces of compound **5e**.

To determine the conformational stability of compounds at the PARP1 binding site, MD simulations are employed to assess structural and dynamic changes throughout the protein–ligand interactions [37]. The complex structures are solved using orthorhombic simple point charge (SPC) water models. On periodic boundary conditions, the system was determined to have a cut-off for Lennard–Jones interactions of 10 Å. In the integration steps, a time step of 2.0 fs was used. The system temperature and pressure were set to 300 K and 1.01325 bar, respectively, using the Nose–Hoover thermostat and Martyna–Tobias–Klein protocols. Before the production run, the system was minimized, equilibrated, and 100 ns MD simulations were then performed [38].

2.6. Bioinformatic Analysis of the Binding of Compound 5e towards the Catalytical Grove of PARP1

Compound **5e** was studied using molecular docking modeling to assess the binding of compound **5e** towards the catalytical grove of PARP1 [39]. Figure 6A depicts the binding pose of compound **5e** with PARP1. Docking simulations revealed the prominent interactions of compound **5e** with PARP1 active site residues (Figure 6B). The docking score was assigned to compound **5e** that binds to the active site with −7.33 kcal/mol energy and forms potential hydrogen bonds. TYR49 is bonded with the nitrogen of the pyrimidine ring and ARG217 with the oxygen of methoxybenzene with the bond distances 2.50 and 3.56 Å (Figure 7), respectively. Furthermore, pi–pi stacking interactions exist with ILE218 and TYR235. In addition to the latter, hydrophobic interactions have been discovered in the active site [39]. 100 ns MD simulations were run for the molecule in the PARP1 binding pocket, and the associated coordinates throughout the MD simulation were gathered separately in the trajectory file. Figure 8 depicts the root-mean-square deviations (RMSDs) of Cα atoms in the investigated systems. After 30 ns of MD simulations, all of the studied systems have relaxed and show no significant fluctuations in RMSD values. The evaluated system exhibited an average RMSD of less than 3.0 Å. The LigFitProt RMSD plot displays the RMSD of ligands when the protein–ligand complex is initially aligned as a reference state with the backbone atoms of the protein.
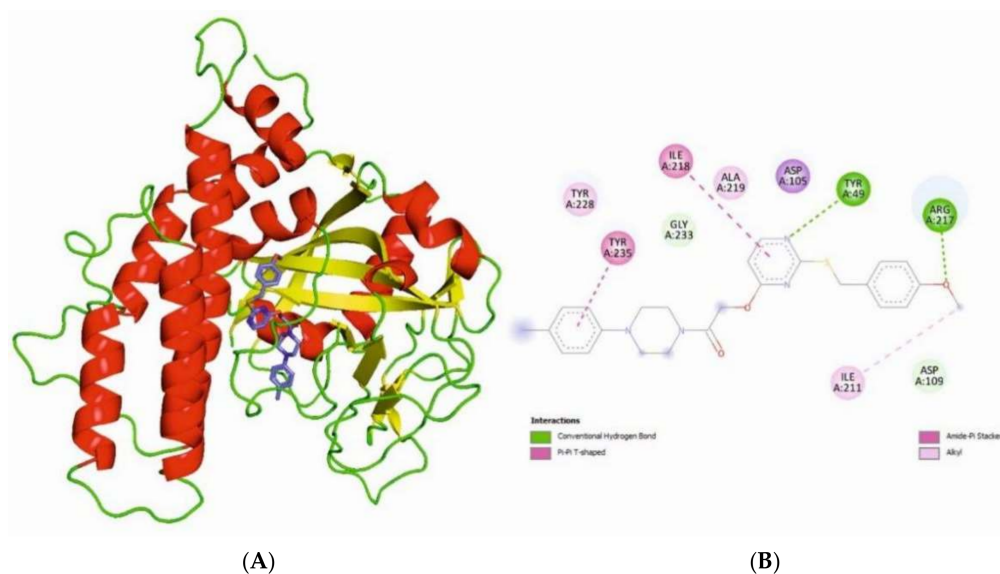
Figure 6. Cartoon representation of PARP1 with compound **5e** (**A**) and its 2D interactions (4HHY) (**B**).
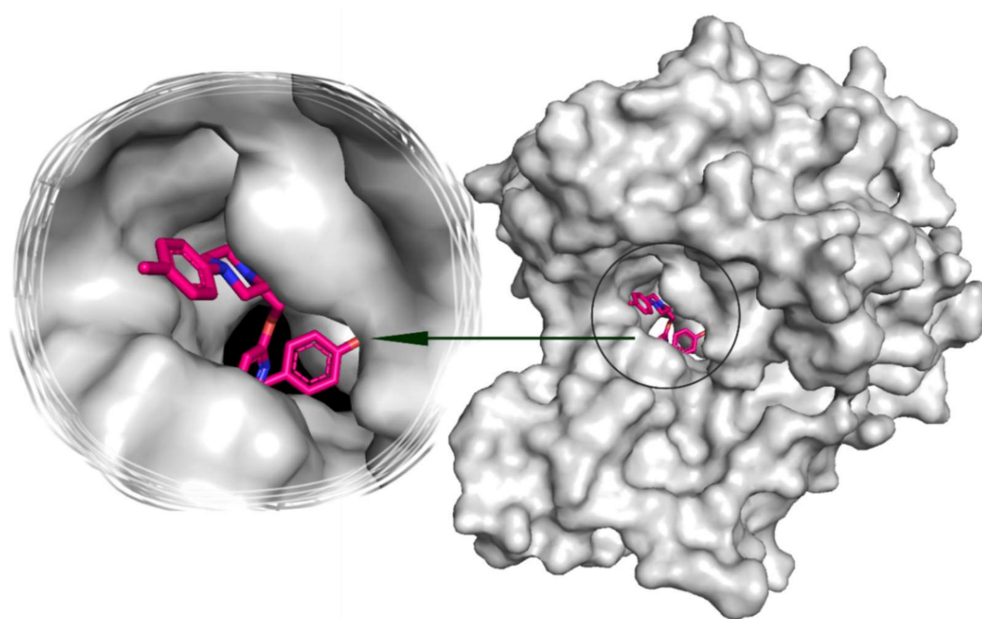
Figure 7. 3D surface view of PARP1 and compound **5e** and a zoomed view of the compound **5e** in the active site cavity.

Root-mean-square fluctuation (RMSF) values were also calculated during simulations to investigate the effect of defined hits on the mobility of the target protein's backbone atoms (Figure 9). Figure 10A depicts associations that appear in the chosen path for more than 6% of the simulation time (0.00–100.00 ns). Hydrogen bonds with TYR49 and π–π stacking interactions with TYR228 produce significant interactions in the molecule. ASP105, ARG217, ALA219, GLY233, and TYR235 have stable non-bonded chemical contacts throughout the simulations, as shown by the protein–ligand interactions graph Figure 10B. The stability between compound **5e** and PARP1 is furthermore enhanced by the interaction with the amino acid residues ARG217, GLY233, ALA219, and TYR49 of PARP1 via water bridges [40].
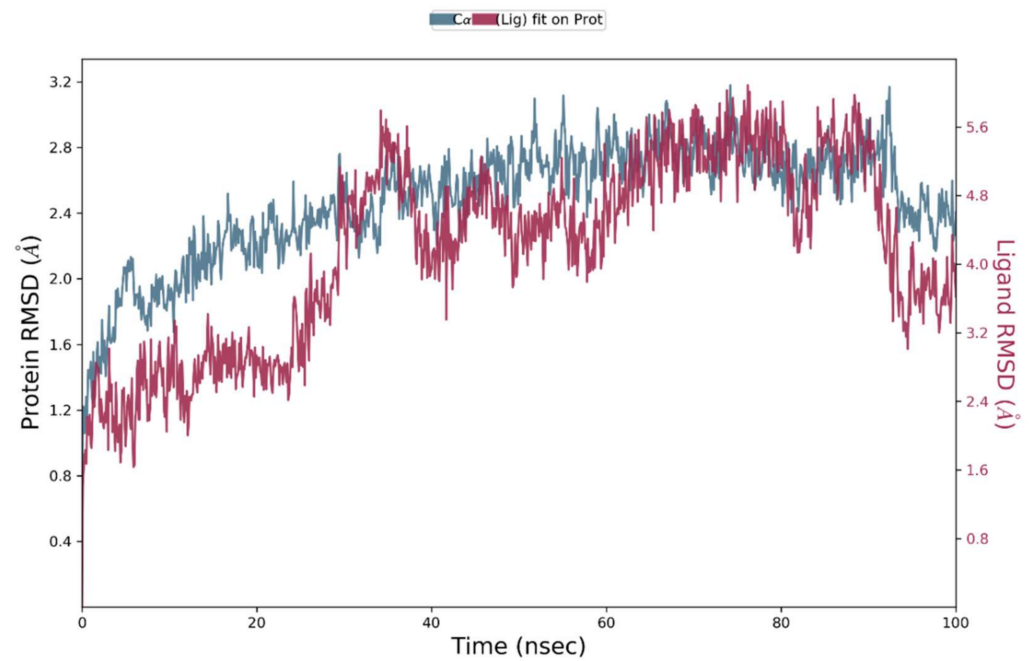
Figure 8. RMSD plot of ligand **5e** and PARP1.
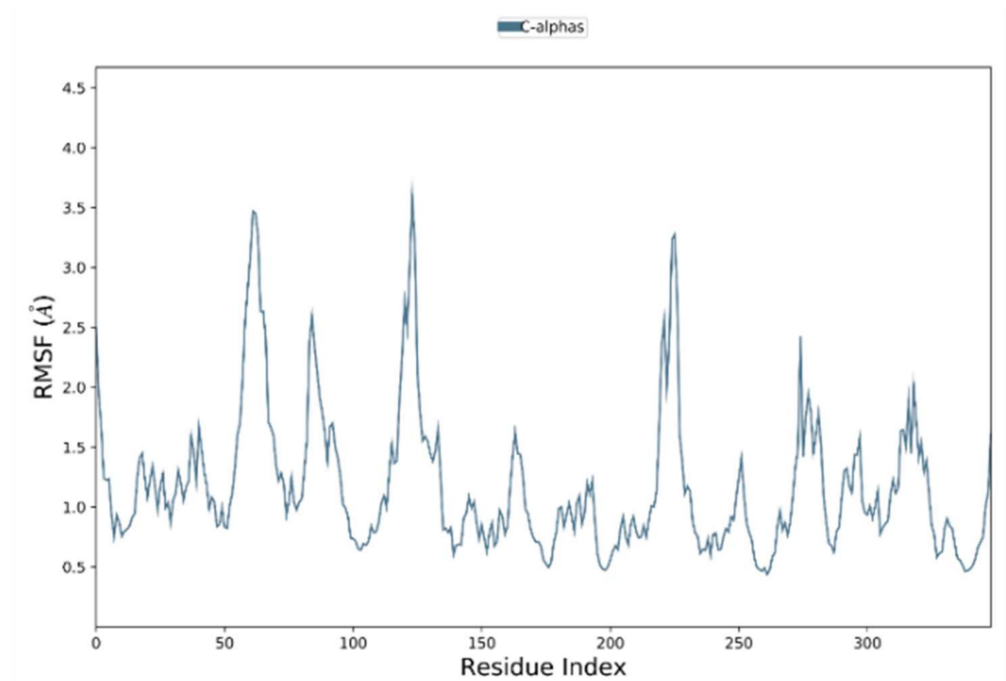
Figure 9. RMSF plot of protein molecule (4HHY) PARP1.
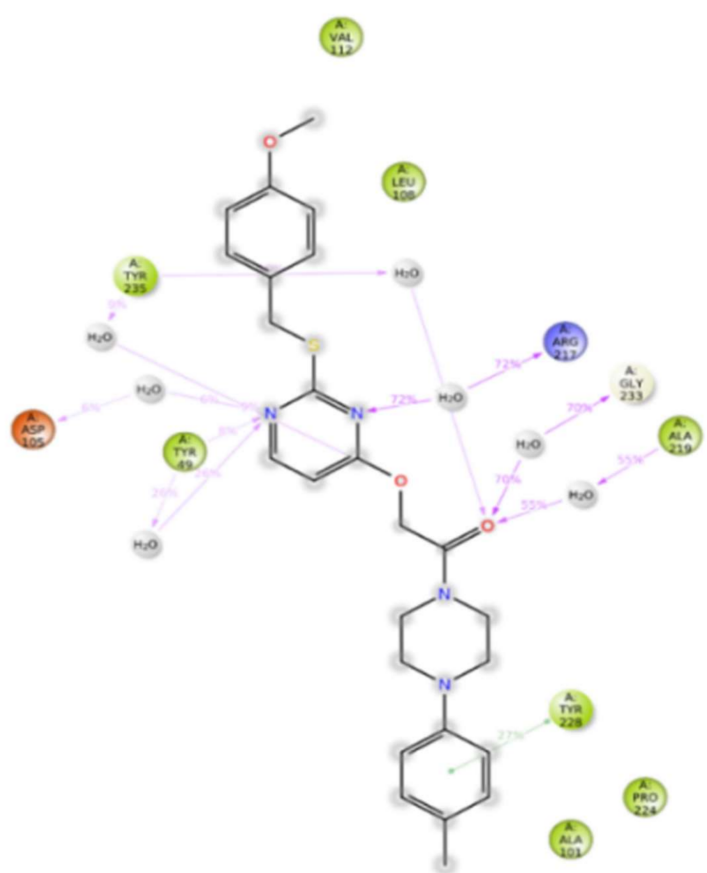
(**a**)
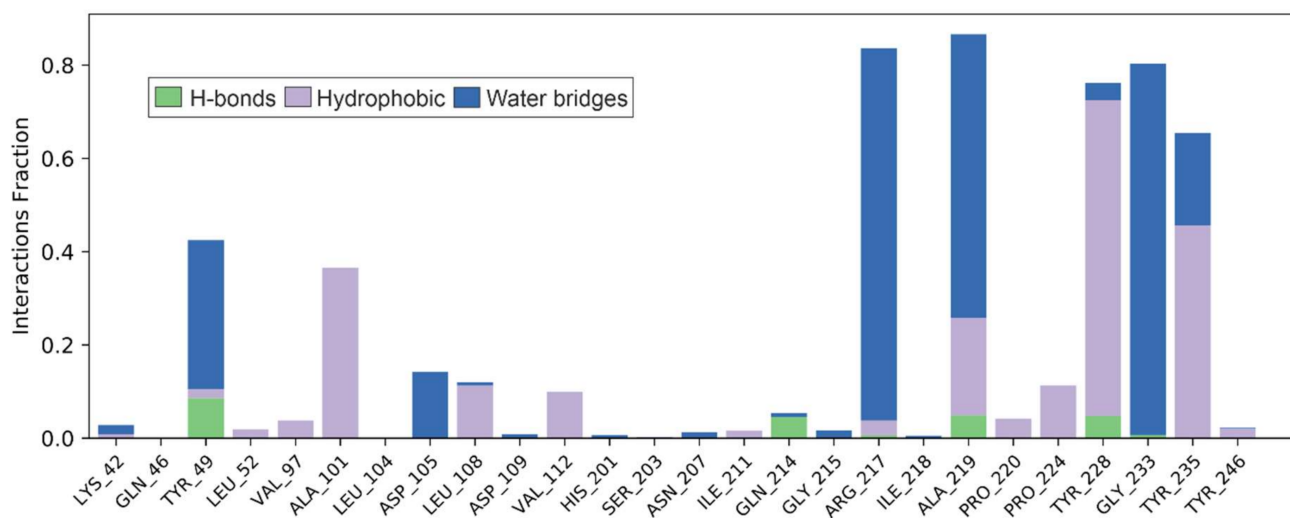
(**b**)

Figure 10. (**a**) Compound **5e**-PARP1 interaction and (**b**) histogram charts of the interaction percentages of the MD simulation for the complex.

3. Materials and Methods

All organic chemicals used were purchased from Sigma-Aldrich. ¹H and ¹³C NMR spectra were recorded on a Bruker WH-200 (400 MHz) and JEOLJSM-ECS (400 MHz) spectrometer in CDCl₃ as solvent, using TMS as an internal standard, and chemical shifts are expressed as ppm. High-resolution mass spectra were determined on a Bruker Daltonics instrument. Mass spectra were determined on an Agilent LC-MS and the elemental analyses were carried out using an Elemental Vario Cube CHNS rapid analyzer. The progress of the reaction was monitored by TLC precoated silica gel G plates [41].

3.1. Synthesis of Compound 2

To a stirred solution of 2-thiouracil, p-methoxy benzyl bromide in DMF was added potassium carbonate, and the reaction mixture was heated to 80 °C. The reaction was monitored by thin-layer chromatography, quenched with water, and extracted with ethyl acetate. The organic layer was washed with brine and dried over sodium sulfate and concentrated under vacuum. The crude product was purified by column chromatography with silica-60 to yield the alcohol **2** in 81% yield.

3.2. Synthesis of Compound 3

To a stirred solution of alcohol **2**, tert-butyl bromoacetate in DMF was added potassium carbonate (1.2 eq), and the reaction mixture was heated to 80 °C. The reaction was monitored by thin-layer chromatography. After completion of the reaction, it was quenched with water and extracted with ethyl acetate. The organic layer was washed with brine and dried over sodium sulfate and concentrated under vacuum. The crude product was purified by column chromatography with silica-60 to afford the ester **3** in 85% yield.

3.3. Synthesis of Compound 4

To a stirred solution of ester **3** in dichloromethane, was added trifluoroacetic acid and stirred overnight. After completion of the reaction as monitored by thin-layer chromatography, it was quenched with sodium bicarbonate and extracted with ethyl acetate. The organic layer was washed with brine and dried over sodium sulfate and concentrated under vacuum. The crude product was purified by column chromatography with silica-60 to afford acid in 65% yield.

3.4. General Synthetic Method for the Preparation of 5a–5l

To a stirred solution of the acid (100 mg, 0.33 mol) in dry dichloromethane (4 mL) under nitrogen atmosphere, was added EDC. HCl (93.7 mg, 0.49 mol). Then, DMAP (4 mg, 10 mol%), amine derivative (130.8 mg, 0.49 mol) was added to the reaction mixture and stirred for five minutes. Triethylamine (0.15 mL, 0.99 mol) was then added slowly, dropwise, to the reaction mixture and it was stirred for 2–3 h. After completion of the reaction, as indicated by TLC, it was quenched with water (5 mL) and extracted with ethyl acetate (2 × 10 mL). The combined organic layers were washed with brine (5 mL) and dried over anhydrous sodium sulfate. Evaporation of the solvent gave the crude residue which was purified by silica gel column chromatography using petroleum ether/EtOAc (3:7) as eluent to furnish amides **5a–5l**.

1-(4-(2,3-Dichlorophenyl)piperazin-1-yl)-2-((2-((4-methoxybenzyl)thio)pyrimidin-4-yl)oxy)ethanone (**5a**), Reddish yellow solid; MP: 145–148 °C; 88% yield; ¹H NMR (400 MHz, CDCl₃): δ 8.29 (d, *J* = 5.6 Hz, 1H), 7.30 (d, *J* = 8.4 Hz, 2H), 7.18 (d, *J* = 8.0 Hz, 1H), 7.11 (t, *J* = 8.0 Hz 1H), 6.83–6.78 (m, 3H), 6.58 (d, *J* = 5.6 Hz, 1H), 5.03 (s, 2H), 4.33 (s, 2H), 3.77 (s, 5H), 3.59 (s, 2H), 3.07 (s, 4H; ¹³C NMR (100 MHz, CDCl₃): δ 173.1, 169.6, 167.3, 160.8, 159.7, 152.3, 150.3, 136.0, 132.0, 130.9, 129.7, 129.4, 127.2, 120.8, 120.5, 115.9, 105.9, 65.0, 57.2, 53.4, 47.1, 44.2, 41.2, 36.8; LCMS (ESI): *m/z* for C₂₄H₂₄Cl₂N₄O₃S+H, calcd 519.0946; found: 519.0929.

1-(4-(3,4-Difluorophenyl)piperazin-1-yl)-2-((2-((4-methoxybenzyl)thio)pyrimidin-4-yl)oxy)ethanone (**5b**), Yellow white solid; MP: 135–138 °C; 92% yield; ¹H NMR (400 MHz, CDCl₃): δ 8.29

(d, *J* = 5.7 Hz, 1H), 7.28 (s, 1H), 7.02 (d, *J* = 9.5 Hz, 2H), 6.80 (d, *J* = 8.5 Hz, 2H), 6.61–6.51 (m, 3H), 5.02 (s, 2H), 4.31 (s, 2H), 3.76 (d, 5H), 3.58 (s, 2H), 3.07 (d, *J* = 16.2 Hz, 4H); ^{13}C NMR (100 MHz, CDCl$_3$): δ 167.8, 165.5, 159, 158.0, 148.0, 130.0, 129.1, 117.5, 114.1, 112.5, 106.3, 104.1, 63.11, 55.2, 50.1, 49.8, 44.8, 41.9, 40.0, 35.1, 22.8; LCMS (ESI): *m/z* for C$_{24}$H$_{24}$F$_2$N$_4$O$_3$S+H, calcd 487.1537; found: 487.0645.

1-(4-(4-Chloro-2-fluorophenyl)piperazin-1-yl)-2-((2-((4-methoxybenzyl)thio)pyrimidin-4-yl)oxy)eth-anone (**5c**), White solid; MP: 142–145 °C; 90% yield; ^{1}H NMR (400 MHz, CDCl$_3$): δ 8.29 (d, *J* = 5.6 Hz, 1H), 7.28 (d, *J* = 24.8 Hz, 2H), 7.05 (dd, *J* = 12, 2.4 Hz, 1H), 6.97 (d, *J* = 8.4 Hz, 1H) 6.82 (d, *J* = 8.8 Hz, 2H), 6.73 (m,1H), 6.58 (d, *J* = 5.6 Hz, 1H), 5.02 (s, 2H), 4.31 (s, 2H), 3.77 (s, 5H), 3.58 (m, 2H), 3.01 (m, 4H); ^{13}C NMR (100 MHz, CDCl$_3$): 171.2, 167.7, 165.3, 158.9, 157.8, 156.6, 154.1, 138.3, 138.2, 130.0, 129.0, 124.6, 124.5, 120.0, 117.1, 116.8, 114.0, 104.0, 63.0, 55.2, 50.7, 50.2, 42.0, 34.9.; LCMS (ESI): *m/z* for C$_{24}$H$_{24}$ClFN$_4$O$_3$S+H, calcd 503.1242; found: 503.0788.

1-(4-Acetyl-1,4-diazepan-1-yl)-2-((2-((4-methoxybenzyl)thio)pyrimidin-4-yl)oxy)ethanone (**5d**), ^{1}H NMR (400 MHz, CDCl$_3$): δ 8.27 (d, *J* = 5.8 Hz, 1H), 7.29 (d, *J* = 8.4 Hz, 2H), 6.82 (d, *J* = 8.2 Hz, 2H), 6.56 (d, *J* = 5.9 Hz, 1H), 5.00–4.96 (m, 2H), 4.31 (d, *J* = 5.0 Hz, 2H), 3.77 (s, 3H), 3.63–3.47 (m, 8H), 2.07 (d, *J* = 3.4 Hz, 3H), 1.90 (d, *J* = 31.1 Hz, 2H); ^{13}C NMR (100 MHz, CDCl$_3$): δ δ171.2, 170.7, 166.9, 159.1, 157.7, 130.1, 129.3, 114.1, 104.2, 63.2, 62.9, 55.4, 49.2, 48.6, 45.1,44.4, 34.9; LCMS (ESI): *m/z* for C$_{21}$H$_{26}$N$_4$O$_4$S+H, calcd 431.1675; found: 431.0702.

2-((2-((4-Methoxybenzyl)thio)pyrimidin-4-yl)oxy)-1-(4-(p-tolyl)piperazin-1-yl)ethanone (**5e**), ^{1}H NMR (400 MHz, CDCl$_3$): δ 8.29 (d, *J* = 5.6 Hz, 1H), 7.29 (d, *J* = 16.0 Hz, 2H), 7.07 (d, *J* = 8.0 Hz, 2H), 6.87–6.74 (m, 4H), 6.57 (d, *J* = 5.6 Hz, 1H), 5.03 (s, 2H), 4.32 (s, 2H), 3.78 (s, 5H), 3.57 (S, 2H), 3.16–3.02 (m, 4H), 2.28 (s, 3H); ^{13}C NMR (100 MHz, CDCl$_3$): δ 171.4, 167.9, 165.5, 159.0, 157.9, 130.5, 130.2 129.9, 117.4, 114.1, 104.1, 63.3, 55.4, 50.4, 50.1, 45.0, 42.1, 35.0, 20.6; LCMS (ESI): *m/z* for C$_{25}$H$_{28}$N$_4$O$_3$S+H, calcd 465.1882; found: 465.0852.

1-(4-(2-Fluorophenyl)piperazin-1-yl)-2-((2-((4-methoxybenzyl)thio)pyrimidin-4-yl)oxy)ethanone (**5f**), ^{1}H NMR (400 MHz, CDCl$_3$): δ 8.28 (d, *J* = 5.6 Hz, 1H), 7.29 (d, *J* = 8.8 Hz, 2H), 7.05–6.94 (m, 4H), 6.86–6.81 (m, 3H), 6.57 (d, *J* = 5.6 Hz, 1H), 5.03 (s, 2H), 4.32 (s, 2H), 3.77 (s, 5H), 3.58 (s, 2H), 3.12–3.02 (m, 4H); ^{13}C NMR (100 MHz, CDCl$_3$): δ 171.2, 167.8, 165.3, 158.8, 157.8, 157.0, 139.4, 139.3, 130.1, 130.0, 129.5, 128.5, 125.1, 123.3, 119.3, 117.6, 116.3, 113.5, 103.5, 68.1, 63.1, 55.3, 50.8, 50.3, 45.0, 42.1, 34.8; LCMS (ESI): *m/z* for C$_{24}$H$_{25}$FN$_4$O$_3$S+H, calcd 469.1631; found: 469.2454.

2-((2-((4-Methoxybenzyl)thio)pyrimidin-4-yl)oxy)-N-(5-(trifluoromethyl)-1,3,4-thiadiazol-2-yl)acet-amide (**5g**), ^{1}H NMR (400 MHz, CDCl$_3$): δ 8.33 (d, *J* = 5.3 Hz, 1H), 7.18 (d, *J* = 8.0 Hz, 2H), 6.74 (d, *J* = 8.0 Hz, 2H), 6.62 (d, *J* = 5.4 Hz, 1H), 5.21 (s, 2H), 4.23 (s, 2H), 3.73 (s, 3H); ^{13}C NMR (100 MHz, CDCl$_3$): δ 171.1, 166.6, 166.4, 161.0, 158.3, 157.7, 129.5, 129.3, 128.2, 113.4, 103.4, 63.6, 54.7, 34.2; LCMS (ESI): *m/z* for C$_{17}$H$_{14}$F$_3$N$_5$O$_3$S$_2$+H, calcd 458.0490; found: 458.1220.

N-(Furan-2-ylmethyl)-2-((2-((4-methoxybenzyl)thio)pyrimidin-4-yl)oxy)acetamide (**5h**), ^{1}H NMR (400 MHz, CDCl$_3$): δ 8.29 (d, *J* = 5.6 Hz, 1H), 7.40–7.26 (m, 3H), 6.83 (d, *J* = 8 Hz, 2H), 6.58 (brs, 1H), 6.48 (d, *J* = 6.0 Hz, 1H), 6.32 (s, 1H), 6.24 (s, 1H), 4.86 (s, 2H), 4.51 (d, *J* = 5.6 Hz, 2H), 4.31 (s, 2H), 3.78 (s, 3H); ^{13}C NMR (100 MHz, CDCl$_3$): δ 172.1, 167.0, 158.8, 158.1, 150.6, 142.3, 130.8, 130.1, 1291, 128.8, 114.5, 110.5, 107.7, 103.4, 68.1, 64.8, 55.2, 36.0, 34.8; LCMS (ESI): *m/z* for C$_{19}$H$_{19}$N$_3$O$_4$S+H, calcd 386.1096; found: 386.1792.

2-((2-((4-Methoxybenzyl)thio)pyrimidin-4-yl)oxy)-N-(1,2,3,4-tetrahydronaphthalen-1-yl)acetamide (**5i**), ^{1}H NMR (400 MHz, CDCl$_3$): δ 8.27 (d, *J* = 5.7 Hz, 1H), 7.70 (dd, *J* = 5.7, 3.3 Hz, 1H), 7.53 (dd, *J* = 5.7, 3.3 Hz, 1H), 7.34 (d, *J* = 8.6 Hz, 2H), 7.18 (s, 1H), 7.11 (s, 1H), 6.85 (d, *J* = 8.6 Hz, 2H), 6.44 (d, *J* = 5.7 Hz, 1H), 4.89 (d, *J* = 3.5 Hz, 2H), 4.35 (s, 2H), 4.22 (m,1H), 3.78 (s, 3H), 2.79 (dd, *J* = 12.4, 5.9 Hz, 2H), 1.81 (dd, *J* = 12.0, 6.7 Hz, 4H); ^{13}C NMR (100 MHz, CDCl$_3$): δ 171.9, 167.7, 167.1, 166.6, 158.8, 158.0, 137.63, 136.1, 130.84, 130.0, 129.2, 129.0, 128.43, 128.4, 128.2, 127.4, 126.4, 113.9, 103.5, 68.1, 55.3, 47.3, 38.7, 34.9, 20.1.

2-((2-((4-Chlorobenzyl)thio)-6-methylpyrimidin-4-yl)oxy)-1-(4-(3,4-dichlorophenyl)piperazin-1-yl)ethan-1-one (**5j**), Off white solid; MP: 135–138 °C; 88% yield; ^{1}H NMR (400 MHz, CDCl$_3$): δ 7.32 (d, *J* = 8.4 Hz, 2H), 7.24 (d, *J* = 8.2 Hz, 2H), 7.19 (dd, *J* = 8.0, 1.1 Hz, 1H), 7.10 (t, *J* = 8.0 Hz, 1H), 6.80 (dd, *J* = 8.0, 1.1 Hz, 1H), 6.42 (s, 1H), 4.99 (s, 2H), 4.32 (s, 2H), 3.76 (s, 2H), 3.57 (s, 2H), 3.03–2.94 (m, 4H), 2.38 (s, 3H); ^{13}C NMR (100 MHz, CDCl$_3$): δ 169.8, 168.4, 165.6, 150.3, 136.4, 134.2, 133.0, 131.1, 130.1, 128.2, 127.8, 127.5, 125.3, 118.8, 102.7, 63.1, 51.2, 50.9, 50.7, 45.1, 42.2, 34.5, 30.3, 23.8. LCMS (ESI): m/z for C$_{24}$H$_{23}$Cl$_3$N$_4$O$_2$S, calcd 537.8890; found:537.0455.

1-(4-(4-Chlorophenyl)piperazin-1-yl)-2-((2-((4-fluorobenzyl)thio)-6-methylpyrimidin-4-yl)oxy)ethanone (**5k**), Off white solid; MP: 138–142 °C; 90% ^{1}H NMR (400 MHz, CDCl$_3$): δ 7.34 (dd, *J* = 8.1, 5.6 Hz, 2H), 7.22 (d, *J* = 8.8 Hz, 2H), 6.96 (t, *J* = 8.6 Hz, 2H), 6.82 (d, *J* = 8.5 Hz, 2H), 6.43 (s, 1H), 5.00 (s, 2H), 4.32 (s, 2H), 3.75 (s, 2H), 3.59 (s, 2H), 3.12 (d, *J* = 20.8 Hz, 4H), 2.40 (s, 3H). LCMS (ESI): m/z for C$_{24}$H$_{24}$ClFN$_4$O$_2$S, calcd 486.9894; found: 487.1152.

2-((2-((4-Fluorobenzyl)thio)-6-methylpyrimidin-4-yl)oxy)-1-(4-(p-tolyl)piperazin-1-yl)ethanone (**5l**), Yellowish white solid; MP: 134–137 °C; 88% yield; ^{1}H NMR (400 MHz, CDCl$_3$): δ 7.35 (dd, *J* = 8.4, 5.5 Hz, 2H), 7.09 (d, *J* = 8.3 Hz, 2H), 6.96 (t, *J* = 8.6 Hz, 2H), 6.83 (d, *J* = 5.1 Hz, 2H), 6.43 (s, 1H), 5.01 (s, 2H), 4.33 (s, 2H), 3.76 (s, 2H), 3.59 (s, 2H), 3.10 (d, *J* = 17.7 Hz, 4H), 2.40 (s, 3H), 2.29 (s, 3H). LCMS (ESI): m/z for C$_{25}$H$_{27}$FN$_4$O$_2$S, calcd 466.5709; found: 467.1684.

3.5. Cell Viability Assay

MCF-7 and MCF-10A cells were procured from Procell Life Science and Technology Co. LTD, China. Cells (2000) were cultured in MEM or Leibovitz's L-15 medium enriched with 2% FBS, MCF-10A cells were cultured in DMEM with 5% horse serum (HS) (general culture: 2% HS was used for experimental conditions), 20 ng/mL EGF, 0.5µg/mL hydrocortisone, 10µg/mL insulin, 1% NEAA (non-essential amino acids); and maintained in a humidified atmosphere of 5% CO$_2$ at 37 °C. DMSO-dissolved compounds were stored as a stock solution, and diluted with cell culture medium as required. Cells (4×10^3) were cultured for 12 h in 96-well plates and treated with thiouracil amides or Olaparib at 0, 0.01, 0.1, 10, 100, and 1000 µM concentrations for 72 h. The inhibitory effect of the compounds was assessed using Alamar Blue [42–45].

3.6. Assay of PARP1 Catalytic Activity

The catalytic activity of PARP1 was determined using the PARP/Apoptosis Universal Colorimetric Assay Kit (4677-096-K, R&D Systems Ltd., Abingdon, UK) [46]. Compounds **5a** or **5e** or Olaparib were added to recombinant human PARP enzyme prior to evaluation as per manufacturer's instructions.

3.7. Western Blot Analysis

Western blot analysis was performed to determine the levels of cleaved PARP1, and the phosphorylation ofH2AX in MCF-7 cells using previously reported methods [29]. Cells at 50–60% confluence were treated with compounds and incubated for 60 h in 2% FBS. MCF-7 cells were also treated with Olaparib, **5a**, or **5e,** and the levels of cleaved PARP1 and the phosphorylation of p-H2AX were determined using the respective antibodies, as previous [29].

3.8. CASPASE-3/7 Activity Assay

CASPASE-3/7 activity was determined by the Caspase-Glo® 3/7 assay kit (Promega corporation, Madison, WI, USA) according to the manufacturer's instructions [30]. MCF-7 cells were seeded in 96-well plates and incubated overnight. Compounds or vehicle were added to cells after 12 h. After a 24 h incubation period, Caspase-Glo® 3/7 reagent and media (1:1) were added into each well and processed according to the manufacturer's instructions.

3.9. DFT Calculations for the Compound 5e

Computational DFT studies for the **5e** molecule were performed using Gaussian09 [47]. The molecule was built and visualized by Gaussview 5 program package. The molecular geometry of the **5e** molecule was optimized at B3LYP (Becke's three parameter (B3)) level with a 6-311+G (d,p) basis set [48].

3.10. Bioinformatics Studies for the Compound 5e

The Scripps Research Institute's AutoDock Tools (ADT) (v1.5.7) [49,50] was used to generate grid and docking parameter files.The crystal structure of PARP1 with the ligand was used to retrieve the crystal structure of PARP1 with a ligand (PDB ID: 4HHY) and use it as afor the docking purpose (PDB ID: 4HHY). With the centroid rendered from inhibitor in the crystallographic structure, the grid box size of $65 \times 65 \times 65$ Å with 0.481 Å spacing is defined. The empirical free-energy function and the Lamarckian genetic algorithm were used to perform molecular docking with the macromolecule, with an initial population of 150 randomly placed individuals, a maximum number of 2,500,000 energy evaluations, a mutation rate of 0.02, a crossover rate of 0.80, and 10 docking runs. Visualization plots were examined using BIOVIA Discovery Studio Visualizer (v21.10.20298) [51] and PyMOL (v2.5.2) [52,53].

3.11. Statistical Analysis

The data were analyzed by Student's *t*-test and $p < 0.05$ was considered statistically significant (GraphPad Prism 5.0; GraphPad Software, La Jolla, CA, USA).

4. Conclusions

A series of thiouracil derivatives containing amide linkages were synthesized and screened for loss of viability of breast cancer cells. The compounds exhibited moderate to significant activity in MCF-7 cells. Compounds **5a** and **5e** inhibited PARP1 activity, produced PARP cleavage, and enhanced phosphorylation of H2AX. Computational methodologies demonstrated conclusively that compound **5e** interacts with PARP.

References

1. Sonnenblick, A.; de Azambuja, E.; Azim, H.A., Jr.; Piccart, M. An update on PARP inhibitors—moving to the adjuvant setting. *Nat. Rev. Clin. Oncol.* **2015**, *12*, 27–41. [CrossRef] [PubMed]
2. Beck, C.; Robert, I.; Reina-San-Martin, B.; Schreiber, V.; Dantzer, F. Poly(ADP-ribose) polymerases in double-strand break repair: Focus on PARP1, PARP2 and PARP3. *Exp. Cell Res.* **2014**, *329*, 18–25. [CrossRef] [PubMed]
3. Kim, M.Y.; Zhang, T.; Kraus, W.L. Poly(ADP-ribosyl)ation by PARP-1, 'PAR-laying' NAD+ into a nuclear signal. *Genes Dev.* **2005**, *19*, 1951–1967. [CrossRef]
4. Kraus, W.L. Transcriptional control by PARP-1, chromatin mod-ulation, enhancer-binding, coregulation, and insulation. *Curr. Opin. Cell Biol.* **2008**, *20*, 294–302. [CrossRef]
5. Oza, A.M.; Tinker, A.V.; Oaknin, A.; Shapira-Frommer, R.; McNeish, I.A.; Swisher, E.M.; Ray-Coquard, I.; Bell-McGuinn, K.; Coleman, R.L.; O'Malley, D.M.; et al. Antitumor activity and safety of the PARP inhibitor rucaparib in patients with high-grade ovarian carcinoma and a germline or somatic BRCA1 or BRCA2 mutation: Integrated analysis of data from study 10 and ARIEL2. *Gynecol. Oncol.* **2017**, *147*, 267–275. [CrossRef]
6. Kaye, S.B.; Lubinski, J.; Matulonis, U.; Ang, J.E.; Gourley, C.; Karlan, B.Y.; Amnon, A.; Bell-McGuinn, K.M.; Chen, L.M.; Friedlander, M.; et al. Phase II, open-label, randomized, multi- center study comparing the efficacy and safety of olaparib, a poly (ADP-ribose) polymerase inhibitor, and pegylated liposomal doxorubicin in patients with BRCA1 or BRCA2 mutations and recurrent ovarian cancer. *J. Clin. Oncol.* **2012**, *30*, 372–379. [CrossRef]
7. Litton, J.K.; Rugo, H.S.; Ettl, J.; Hurvitz, S.A.; Gonçalves, A.; Lee, K.-H.; Fehrenbacher, L.; Yerushalmi, R.; Mina, L.A.; Martin, M.; et al. Talazoparib in patients with advanced breast cancer and a germline BRCA mutation. *N. Engl. J. Med.* **2018**, *379*, 753–763. [CrossRef]
8. Swisher, E.M.; Lin, K.K.; Oza, A.M.; Scott, C.L.; Giordano, H.; Sun, J.; Konecny, G.E.; Coleman, R.L.; Tinker, A.V.; O'Malley, D.M.; et al. Rucaparib in relapsed, platinum-sensitive high-grade ovarian carcinoma (ARIEL2 Part 1): An international, multicentre, open-label, phase 2 trial. *Lancet Oncol.* **2017**, *18*, 75–87. [CrossRef]
9. Schiewer, M.J.; Knudsen, K.E. Transcriptional roles of parp1 in cancer. *Mol. Cancer Res.* **2014**, *12*, 1069–1080. [CrossRef]
10. Zhang, F.; Wang, Y.; Wang, L.; Luo, X.; Huang, K.; Wang, C.; Du, M.; Liu, F.; Luo, T.; Huang, D.; et al. Poly(adp-ribose) polymerase 1 is a key regulator of estrogen receptor alpha-dependent gene transcription. *J. Biol. Chem.* **2013**, *288*, 11348–11357. [CrossRef]
11. Purnell, M.R.; Whish, W.J. Novel inhibitors of poly(ADP-ribose) synthetase. *Biochem. J.* **1980**, *185*, 775–777. [CrossRef] [PubMed]
12. Du, Y.; Yamaguchi, H.; Wei-Chao, C.; Hsu, J.L.; Wang, H.-L.; Hsu, Y.-H.; Lin, W.-C.; Yu, W.-H.; Leonard, P.G.; Lee, G.R., 4th; et al. Blocking c-Met-mediated PARP1 phosphorylation enhances anti-tumor effects of PARP inhibitors. *Nat. Med.* **2016**, *22*, 194–201. [CrossRef] [PubMed]
13. National Center for Biotechnology Information. PubChem Patent Summary for US-8071623-B2. 2022. Available online: https://pubchem.ncbi.nlm.nih.gov/patent/US-8071623-B2 (accessed on 12 January 2022).
14. Berger, S.H.; Pittman, D.L.; Wyatt, M.D. Uracil in DNA: Consequences for carcinogenesis and chemotherapy. *Biochem. Pharmacol.* **2008**, *76*, 697–706. [CrossRef] [PubMed]
15. Steinhagen, H.; Gerisch, M.; Mittendorf, J.; Schlemmer, K.-H.; Albrecht, B. Substituted uracil derivatives as potent inhibitors of poly(ADP-ribose)polymerase-1 (PARP-1). *Bioorganic Med. Chem. Lett.* **2002**, *12*, 3187–3190. [CrossRef]
16. Weeks, L.; Zentner, G.; Scacheri, P.C.; Gerson, S.L. Uracil DNA glycosylase (UNG) loss enhances DNA double strand break formation in human cancer cells exposed to pemetrexed. *Cell Death Dis.* **2014**, *5*, e1045. [CrossRef]
17. Pandey, V.; Wang, B.; Mohan, C.D.; Raquib, A.R.; Rangappa, S.; Srinivasa, V.; Fuchs, J.E.; Girish, K.S.; Zhu, T.; Bender, A.; et al. Discovery of a small-molecule inhibitor of specific serine residue BAD phosphorylation. *Proc. Natl. Acad. Sci. USA* **2018**, *115*, E10505–E10514. [CrossRef]
18. Zhang, M.; Wang, B.; Chong, Q.-Y.; Pandey, V.; Guo, Z.; Chen, R.-M.; Wang, L.; Wang, Y.; Ma, L.; Kumar, A.P.; et al. A novel small-molecule inhibitor of trefoil factor 3 (TFF3) potentiates MEK1/2 inhibition in lung adenocarcinoma. *Oncogenesis* **2019**, *8*, 65. [CrossRef]
19. Sulaiman, N.B.S.; Mohan, C.D.; Basappa, S.; Pandey, V.; Rangappa, S.; Bharathkumar, H.; Kumar, A.P.; Lobie, P.E.; Rangappa, K.S. An azaspirane derivative suppresses growth and induces apoptosis of ER-positive and ER-negative breast cancer cells through the modulation of JAK2/STAT3 signaling pathway. *Int. J. Oncol.* **2016**, *49*, 1221–1229. [CrossRef]
20. Basappa; Sugahara, K.; Thimmaiah, K.N.; Bid, H.K.; Houghton, P.J.; Rangappa, K.S. Anti-tumor activity of a novel HS-mimetic-vascular endothelial growth factor binding small molecule. *PLoS ONE* **2012**, *7*, e39444. [CrossRef]
21. Bharathkumar, H.; Mohan, C.D.; Rangappa, S.; Kang, T.; Keerthy, H.K.; Fuchs, J.E.; Kwon, N.H.; Bender, A.; Kim, S.; Basappa, B.; et al. Screening of quinoline, 1,3-benzoxazine, and 1,3-oxazine-based small molecules against isolated methionyl-tRNA synthetase and A549 and HCT116 cancer cells including an in silico binding mode analysis. *Org. Biomol. Chem.* **2015**, *13*, 9381–9387. [CrossRef]
22. Baburajeev, C.P.; Mohan, C.D.; Rangappa, S.; Mason, D.J.; Fuchs, J.E.; Bender, A.; Barash, U.; Vlodavsky, I.; Basappa; Rangappa, K.S. Identification of Novel Class of Triazolo-Thiadiazoles as Potent Inhibitors of Human Heparanase and their Anticancer Activity. *BMC Cancer* **2017**, *17*, 235. [CrossRef] [PubMed]
23. Vishwanath, D.; Girimanchanaika, S.S.; Dukanya, D.; Rangappa, S.; Yang, J.-R.; Pandey, V.; Lobie, P.E.; Basappa, B. Design and Activity of Novel Oxadiazole Based Compounds That Target Poly(ADP-ribose) Polymerase. *Molecules* **2022**, *27*, 703. [CrossRef] [PubMed]

24. Ji, J.; Zhang, Y.; Redon, C.E.; Reinhold, W.C.; Chen, A.P.; Fogli, L.K.; Holbeck, S.L.; Parchment, R.E.; Hollingshead, M.; Tomaszewski, J.E.; et al. Phosphorylated fraction of H2AX as a measurement for DNA damage in cancer cells and potential applications of a novel assay. *PLoS ONE* **2017**, *12*, e0171582. [CrossRef] [PubMed]

25. Mohan, C.D.; Anilkumar, N.C.; Rangappa, S.; Shanmugam, M.K.; Mishra, S.; Chinnathambi, A.; Alharbi, S.A.; Bhattacharjee, A.; Sethi, G.; Kumar, A.P.; et al. Novel 1,3,4-Oxadiazole Induces Anticancer Activity by Targeting NF-κB in Hepatocellular Carcinoma Cells. *Front. Oncol.* **2018**, *8*, 42. [CrossRef] [PubMed]

26. Lee, J.H.; Rangappa, S.; Mohan, C.D.; Basappa; Sethi, G.; Lin, Z.-X.; Rangappa, K.S.; Ahn, K.S. Brusatol, a Nrf2 Inhibitor Targets STAT3 Signaling Cascade in Head and Neck Squamous Cell Carcinoma. *Biomolecules* **2019**, *9*, 550. [CrossRef] [PubMed]

27. Lee, J.H.; Mohan, C.D.; Basappa, S.; Rangappa, S.; Chinnathambi, A.; Alahmadi, T.A.; Alharbi, S.A.; Kumar, A.P.; Sethi, G.; Ahn, K.S.; et al. The IκB Kinase Inhibitor ACHP Targets the STAT3 Signaling Pathway in Human Non-Small Cell Lung Carcinoma Cells. *Biomolecules* **2019**, *9*, 875. [CrossRef]

28. Zeng, X.; Jiang, S.; Ruan, S.; Guo, Z.; Guo, J.; Liu, M.; Ye, C.; Dong, J. MAPK4 silencing together with a PARP1 inhibitor as a combination therapy in triple-negative breast cancer cells. *Mol. Med. Rep.* **2021**, *24*, 548. [CrossRef]

29. Ke, B.; Li, A.; Fu, H.; Kong, C.; Liu, T.; Zhu, Q.; Zhang, Y.; Zhang, Z.; Chen, C.; Jin, C. PARP-1 inhibitors enhance the chemosensitivity of leukemia cells by attenuating NF-κB pathway activity and DNA damage response induced by Idarubicin. *Acta Biochim. Biophys. Sin.* **2022**, *54*, 1–8. [CrossRef]

30. Bhat, A.; Tan, V.; Heng, B.; Chow, S.; Basappa, S.; Essa, M.M.; Chidambaram, S.B.; Guillemin, G.J. Papaverine, a Phosphodiesterase 10A Inhibitor, Ameliorates Quinolinic Acid-Induced Synaptotoxicity in Human Cortical Neurons. *Neurotox Res.* **2021**, *39*, 1238–1250. [CrossRef]

31. Baburajeev, C.P.; Mohan, C.D.; Ananda, H.; Rangappa, S.; Fuchs, J.E.; Jagadish, S.; Siveen, K.S.; Chinnathambi, A.; Alharbi, S.A.; Zayed, M.E.; et al. Development of Novel Triazolo-Thiadiazoles from Heterogeneous "Green" Catalysis as Protein Tyrosine Phosphatase 1B Inhibitors. *Sci. Rep.* **2015**, *5*, 14195. [CrossRef]

32. Naveenkumar, S.K.; Thushara, R.M.; Sundaram, M.S.; Hemshekhar, M.; Paul, M.; Thirunavukkarasu, C.; Basappa; Nagaraju, G.; Raghavan, S.C.; Girish, K.S.; et al. Unconjugated Bilirubin exerts Pro-Apoptotic Effect on Platelets via p38-MAPK activation. *Sci. Rep.* **2015**, *5*, 15045. [CrossRef] [PubMed]

33. Chumadathil Pookunoth, B.; Eshwar Rao, S.; Deveshegowda, S.N.; Kashinath Metri, P.; Fazl-Ur-Rahman, K.; Periyasamy, G.; Virupaiah, G.; Priya, B.S.; Pandey, V.; Lobie, P.E.; et al. Development of a New Arylamination Reaction Catalyzed by Polymer Bound 1,3-(Bisbenzimidazolyl) Benzene Co(II) Complex and Generation of Bioactive Adamanate Amines. *Catalysts* **2020**, *10*, 1315. [CrossRef]

34. Chandramohanadas, R.; Basappa; Russell, B.; Liew, K.; Yau, Y.H.; Chong, A.; Liu, M.; Gunalan, K.; Raman, R.; Renia, L.; et al. Small molecule targeting malaria merozoite surface protein-1 (MSP-1) prevents host invasion of divergent plasmodial species. *J. Infect. Dis.* **2014**, *210*, 1616–1626. [CrossRef] [PubMed]

35. Neelgundmath, M.; Dinesh, K.R.; Mohan, C.D.; Li, F.; Dai, X.; Siveen, K.S.; Paricharak, S.; Mason, D.J.; Fuchs, J.E.; Sethi, G.; et al. Novel synthetic coumarins that targets NF-κB in Hepatocellular carcinoma. *Bioorganic Med. Chem. Lett.* **2015**, *25*, 893–897. [CrossRef] [PubMed]

36. Fleming, I. *Molecular Orbitals and Organic Chemical Reactions*; Wiley: Hoboken, NJ, USA, 2010.

37. Bowers, K.J.; Chow, D.E.; Xu, H.; Dror, R.O.; Eastwood, M.P.; Gregersen, B.A.; Klepeis, J.L.; Kolossvary, I.; Moraes, M.A.; Sacerdoti, F.D.; et al. Scalable algorithms for molecular dynamics simulations on commodity clusters. In Proceedings of the SC'06: 2006 ACM/IEEE Conference on Supercomputing, Tampa, FL, USA, 11–17 November 2006; IEEE: Manhattan, NY, USA, 2006; p. 43.

38. Sahin, K.; Durdagi, S. Identifying new piperazine-based PARP1 inhibitors using text mining and integrated molecular modeling approaches. *J. Biomol. Struct. Dyn.* **2021**, *39*, 681–690. [CrossRef] [PubMed]

39. Khamees, H.A.; Mohammed, Y.H.E.; Ananda, S.; Al-Ostoot, F.H.; Sangappa, Y.; Alghamdi, S.; Khanum, S.A.; Madegowda, M. Effect of o-difluoro and p-methyl substituents on the structure, optical properties and anti-inflammatory activity of phenoxy thiazole acetamide derivatives: Theoretical and experimental studies. *J. Mol. Struct.* **2020**, *1199*, 127024. [CrossRef]

40. Poornima, C.S.; Dean, P.M. Hydration in drug design. 1. Multiple hydrogen-bonding features of water molecules in mediating protein-ligand interactions. *J. Comput. Mol. Des.* **1995**, *9*, 500–512. [CrossRef]

41. Sadashiva, M.P.; Basappa, B.; NanjundaSwamy, S.; Li, F.; Manu, K.A.; Sengottuvelan, M.; Prasanna, D.S.; Anilkumar, N.C.; Sethi, G.; Sugahara, K.; et al. Anti-cancer activity of novel dibenzo[b,f]azepine tethered isoxazoline derivatives. *BMC Chem. Biol.* **2012**, *12*, 5. [CrossRef]

42. Fongmoon, D.; Shetty, A.K.; Basappa; Yamada, S.; Sugiura, M.; Kongtawelert, P.; Sugahara, K. Chondroitinase-mediated Degradation of Rare 3-O-Sulfated Glucuronic Acid in Functional Oversulfated Chondroitin Sulfate K and E. *J. Biol. Chem.* **2007**, *282*, 36895–36904. [CrossRef]

43. Priya, B.; Swamy, S.N.; Tejesvi, M.; Basappa; Sarala, G.; Gaonkar, S.; Naveen, S.; Prasad, J.S.; Rangappa, K. Synthesis, characterization, antimicrobial and single crystal X-ray crystallographic studies of some new sulfonyl, 4-chloro phenoxy benzene and dibenzoazepine substituted benzamides. *Eur. J. Med. Chem.* **2006**, *41*, 1262–1270. [CrossRef]

44. Blanchard, V.; Chevalier, F.; Imberty, A.; Leeflang, B.R.; Basappa; Sugahara, K.; Kamerling, J.P. Conformational studies on five octasaccharides isolated from chondroitin sulfate using NMR spectroscopy and molecular modeling. *Biochemistry* **2007**, *46*, 1167–1175. [CrossRef] [PubMed]

45. Basappa, B.; Pookunoth, B.C.; Kempasiddegowda, M.S.; Subbegowda, R.K.; Lobie, P.; Pandey, V. Novel Biphenyl Amines Inhibit Oestrogen Receptor (ER)-α in ER-Positive Mammary Carcinoma Cells. *Molecules* **2021**, *26*, 783. [CrossRef] [PubMed]

46. Postawski, K.; Monist, M.; Keith, G. PARP-1 activity in normal and cancerous human endometrium and its relationship with quantity of abasic sites (AP). *Ginekol. Pol.* **2011**, *82*, 16–21. [PubMed]

47. Frisch, M.J. *Gaussian 09*; Gaussian Inc.: Wallingford, CT, USA, 2009.

48. El-Remaily, M.A.E.A.A.A.; El-Dabea, T.; Alsawat, M.; Mahmoud, M.H.H.; Alfi, A.A.; El-Metwaly, N.; Abu-Dief, A.M. Development of New Thiazole Complexes as Powerful Catalysts for Synthesis of Pyrazole-4-Carbonitrile Derivatives under Ultrasonic Irradiation Condition Supported by DFT Studies. *ACS Omega* **2021**, *6*, 21071–21086. [CrossRef] [PubMed]

49. El-Remaily, M.A.; Soliman, A.M.; Khalifa, M.E.; El-Metwaly, N.M.; Alsoliemy, A.; El-Dabea, T.; Abu-Dief, A.M. Rapidly, highly yielded and green synthesis of dihydrotetrazolo [1,5-a] pyrimidine derivatives in aqueous media using recoverable Pd (II) thiazole catalyst accelerated by ultrasonic: Computational studies. *Appl. Organomet. Chem.* **2021**, *36*, e6320. [CrossRef]

50. Lee, C.; Yang, W.; Parr, R.G. Development of the Colle-Salvetti correlation-energy formula into a functional of the electron density. *Phys. Rev. B* **1988**, *37*, 785–789. [CrossRef]

51. Sanner, M.F. Python: A programming language for software integration and development. *J. Mol. Graph. Model.* **1999**, *17*, 57–61.

52. BIOVIA Dassault Systèmes. *Discovery Studio Visualizer, 21.1.0.20298*; Dassault Systèmes: San Diego, CA, USA, 2020.

53. Schrödinger, L.; DeLano, W. PyMOL. 2020. Available online: http://www.pymol.org/pymol (accessed on 2 January 2022).